Nuclear Inst. and Methods in Physics Research B 482 (2020) 58–63

Contents lists available at ScienceDirect

Nuclear Inst. and Methods in Physics Research B

journal homepage: www.elsevier.com/locate/nimb

Single-collision scattering of keV-energy Kr ions off a polycrystalline Cu surface

S. Rai[a,b], K.I. Bijlsma[a], S. Koeleman[a], O.G. Tjepkema[a], A.W. Noordam[a], H.T. Jonkman[a], O.O. Versolato[b,c], R. Hoekstra[a,b,*]

[a] Zernike Institute for Advanced Materials, University of Groningen, Nijenborgh 4, 9747 AG Groningen, The Netherlands
[b] Advanced Research Center for Nanolithography (ARCNL), Science Park 106, 1098 XG Amsterdam, The Netherlands
[c] Department of Physics and Astronomy, and LaserLaB, Vrije Universiteit, De Boelelaan 1081, 1081 HV Amsterdam, The Netherlands

ARTICLE INFO

Keywords:
Single-collision scattering
LEIS
SRIM

ABSTRACT

In the keV-energy regime, the scattering of krypton ions off a copper sample has been studied. In addition to the broad energy spectrum arising from multiple-collision scattering, the energy distributions of the backscattered ions exhibit prominent peaks at energies where single-collision (SC) scattering peaks are expected. Such SC peaks were shown to be absent in Sn – Mo/Ru scattering, systems of similar mass ratio and thus similar kinetics. The present Kr on Cu results allow for a comparison to a simulation package as SRIM. An important difference found between the present experiment and the predictions of SRIM is that the SC contribution is observed to decrease with scattering angle, whereas SRIM predicts this contribution to be constant. The intensity of the experimental SC peaks, though much weaker than in the SRIM simulations, may be used as markers to improve SRIM in its description of low-energy heavy particle scattering off surfaces.

1. Introduction

In a recent systematic study [1] of the scattering of keV-energy tin ions from Mo and Ru, materials commonly used in extreme ultraviolet (EUV) optics [2,3], a remarkable observation made was the absence of a single-collision (SC) peak in the energy spectra of the scattered ions. Unlike the experiments, the most widely used package to simulate ion-matter interactions SRIM [4–6] consistently predicted a prominent SC peak on top of the broad distribution of multiple-scattering events. The width and the high-energy shoulder of the multiple-collision feature were found in agreement with the experiments. Series of tests in which the charge state and energy of the incoming Sn ions were changed and the Sn ions replaced by Xe ions, were conducted to investigate this discrepancy. The results led to the conclusion that most likely the SC peak prominently showing up in the SRIM predictions in contrast to the experiments is due to SRIM-related causes such as ignoring any interaction above the surface and using a fixed distance between consecutive collisions. And, perhaps the binary collision approximation underlying SRIM might not be valid anymore for low-energy heavy particle scattering on heavy targets. In any kind of binary collision approximation one expects a SC signature to show up in the energy spectra of scattered particles. A complicating factor in a direct comparison between experiment and SRIM is that SRIM treats all particles as neutral, while experimentally it is most convenient to use ionic beams and to detect scattered charged particles and their energies by means of electrostatic analysers. Ideally one would like to know the ion and neutral fractions, which are however ill-known and depend on energy and surface characteristics. Therefore, Time of Flight (ToF) measurements were performed in which both ions and neutrals are detected [1]. The ToF measurements at a fixed angle supported the finding in the ion spectra that no clear SC peak is detected in the energy spectra of the scattered Sn particles.

Here, we present our followup research on the scattering of keV Kr^+ ions from a polycrystalline Cu sample. We based our choice for the Kr on Cu system on the following arguments. First of all we looked for a collision system with similar single-collision kinetics i.e., similar relative final energy distributions as a function of scattering angle. Within a binary collision approximation the kinetics is governed by the ratio of the target and projectile masses. For Mo or Ru as target and Sn as projectile the mass ratio is ≈0.8. Knowing that for light ion scattering SRIM appears to describe the scattering well, an intermediate-mass collision system seemed appropriate. From the experimental perspective of ion beam production a noble gas is preferred. Therefore the choice was made to use Kr as projectile and with Cu as target a similar

* Corresponding author at: Zernike Institute for Advanced Materials, University of Groningen, Nijenborgh 4, 9747 AG Groningen, The Netherlands.
E-mail address: r.a.hoekstra@rug.nl (R. Hoekstra).

https://doi.org/10.1016/j.nimb.2020.08.021
Received 15 March 2020; Received in revised form 20 August 2020; Accepted 29 August 2020

mass ratio of ≈0.8 is achieved. As will be shown in this paper, in contrast to the case of Sn ion scattering on Mo or Ru, SC peaks do show up in the energy spectra of Kr ions scattered off Cu. This allows us to compare experimental binary collision strengths with ones predicted by the SRIM code as function of scattering angle. This is not possible for the Sn interactions on Mo and Ru as the single-collision peak is absent in the experimental data. The present experimental data on Kr on Cu scattering may assist in improving the SRIM code and evaluating its accuracy in simulating low-energy ion-surface interactions. An improved version of the code will be useful in accurately simulating and predicting the outcome of collisions of Sn ions on Ru-capped multilayer Mo/Si collector mirrors used to collect EUV light used in state-of-the-art nanolithography tools [7,8]. The EUV light is generated by a tin plasma produced by laser irradiation of a stream of molten Sn microdroplets. An unavoidable by-product of such a plasma are fast Sn ions, e.g. [9], which may impact the EUV collector mirrors and reduce collector-mirror lifetime in EUV light sources.

2. Experimental methods

The Kr ion beam is extracted from a SUPERNANOGAN-type electron cyclotron resonance ion source. By means of a 110° analyzing magnet a beam of isotopically pure $^{84}Kr^+$ ions is selected and transported to the collision chamber via a series of three magnetic quadrupole triplets and a 45° dipole magnet in front of the setup for final mass-over-charge clean-up of the beam [1]. Since details of the setup can be found elsewhere e.g., [10–12] only the parts of direct relevance to the present scattering experiments will be recalled briefly. The polycrystalline Cu target is mounted on a high precision manipulator allowing for the adjustment of the angle of incidence (ψ), measured with respect to the surface. In all the experiments a fixed incidence angle of 15° is used.

The kinetic-energy spectra of Kr ions are recorded at scattering angles (θ) ranging from 20° to 40° by means of a rotatable, high precision electrostatic analyzer (ESA) with an opening angle of about 0.3°. The target used in this work is polycrystalline Cu, prepared by Surface Preparation Lab (SPL). ESA spectra as for example shown in Fig. 1 are built up out of a series of kinetic energy scans. For each energy point, the beam current on target is recorded. The typical beam current was 50 nA. Beam fluctuations affect the spectra hence the number of counts per second is divided by the accumulated beam current. Furthermore, because the ESA is operated in fixed $\Delta E/E$ mode the data is corrected for the changing energy-bin width ΔE, by dividing the yield by ΔE. Thereafter, as final correction step, the data is corrected for the energy-dependent detection efficiency of the micro-channel plate [13] used to detect the scattered Kr ions.

For comparison to and interpretation of the experimental data SRIM simulations have been performed. As calculation method we used the *Monolayer Collision Steps/ Surface Sputtering* option of SRIM, which is recommended for ion interactions near the surface [4], although as shown by Deuzeman [1] the differences between the different calculation methods offered by SRIM are very small. For comparison to the experiments, the backscattered particles are required to be in the plane defined by the ion beam and the detector plane within an angular width of 3°. Concerning the in-plane angular acceptance, only particles which are within 1° of a chosen scattering angle are counted. These acceptance angles are larger than the actual ones of the ESA (0.3°). The code was run with the same ^{84}Kr isotope as used in the experiments. For the target sample a mixture of ^{63}Cu and ^{65}Cu isotopes is used in accordance with their natural abundances of 31 and 69%. To obtain sufficient statistics 46.5×10^6 trajectories were calculated in eight batches, each of which used a different random number seed.

Following the binary collision approximation, it is derived that a single collision between a projectile of mass m_p with a kinetic energy E_0 and a target atom of mass m_t leading to scattering over an angle θ results in a final energy of the scattered projectile E_f given by [14]

$$\frac{E_f}{E_0} = \left(\frac{\cos(\theta) + \sqrt{(m_t/m_p)^2 - \sin^2(\theta)}}{1 + m_t/m_p} \right)^2. \quad (1)$$

Apart from the scattered projectiles, recoiled target ions may also end up in the spectra upon a single-collision, at an energy of

$$\frac{E_{rec}}{E_0} = \frac{4 m_t m_p}{(m_t + m_p)^2} \cos^2(\theta). \quad (2)$$

In the energy spectra of scattered ions we indicate the positions of these SC scattering and recoil energies with red and green arrows, respectively. Instead of via a single collision, an ion can also scatter over a certain angle θ via two consecutive collisions. A special case is a symmetric double collision (SDC), i.e. two consecutive collisions over a scattering angle of $\theta/2$. The final energy of such a particle is also denoted in the spectra, with a blue arrow. The energy of the SDC marks the maximum energy which can be attained in a double-collision, all other (asymmetric) double collisions lead to energies in between the SC and SDC energies.

3. Results and discussion

Fig. 1 shows a typical set of energy distributions of 7 keV Kr^+ scattering off a Cu target. As mentioned in the introduction, in the scattered ion spectra of keV-energy Sn ions impinging on Mo and Ru, the SC peaks were absent. However now for Kr^+ on Cu, as Fig. 1 shows, a clear presence of prominent SC peaks is observed. It can also be seen that the energy of SDC is a fair indication of the maximum energy of scattered projectiles.

In the energy spectra (cf. Fig. 1) a small shift between the calculated SC peak positions and the actual measured energies is noted that hints at an offset of 1.1° in the angular position of the ESA. Image charge attraction on the incoming and outgoing trajectories of the ions can at most explain approximately 0.2°, therefore the shift is most likely due to a small 1° offset in the zero-degree calibration of the ESA. In the following, scattering angles are corrected for this 1° offset.

Contributions of Cu recoils to the spectra appear to show up in spectra. However these contributions appear weak and as such do not contribute significantly to the total yield of measured ions. Therefore, they will not be considered separately in the further discussion on the contribution of single-collision scattering to the total yield of backscattered ions.

Similar to Fig. 1, Fig. 2 shows energy spectra of backscattered particles resulting from an SRIM simulation of 46.5 million 7 keV Kr particles impinging on Cu under an incidence angle ψ of 15°. It shows clearly that for scattering angles equal to or exceeding twice the incidence angle a prominent SC peak is present in the synthetic energy spectra. In comparison to the experimental data depicted in Fig. 1 the calculated SC features are much stronger. The SC peak is absent in the SRIM spectra for scattering angles smaller than 30°. This is a known flaw of SRIM stemming from taking a fixed distance between consecutive collisions [1,15]. As is illustrated in the inset of the top-left panel, the first collision in SRIM takes place at a distance d (the mean free path) away from the point where the particle entered the surface. The particle is marked backscattered if it is scattered towards the surface and the subsequent point of collision, at a distance d, would be above the surface. For single-collision scattering this is only possible if the outgoing angle of the projectile, with respect to the target surface, is larger than the incoming angle. Otherwise, the particle is forced to undergo a second collision, thereby inhibiting the occurrence of a SC peak at scattering angles below 2ψ. Therefore, a comparison of experimental and SRIM results regarding SC peak intensities is limited to scattering angles $\theta > 30°$.

Fig. 3 shows the yield of single-collision scattering as a function of scattering angle, obtained from the experimental data as well as from the SRIM simulations. These SC ion yields are determined by assuming

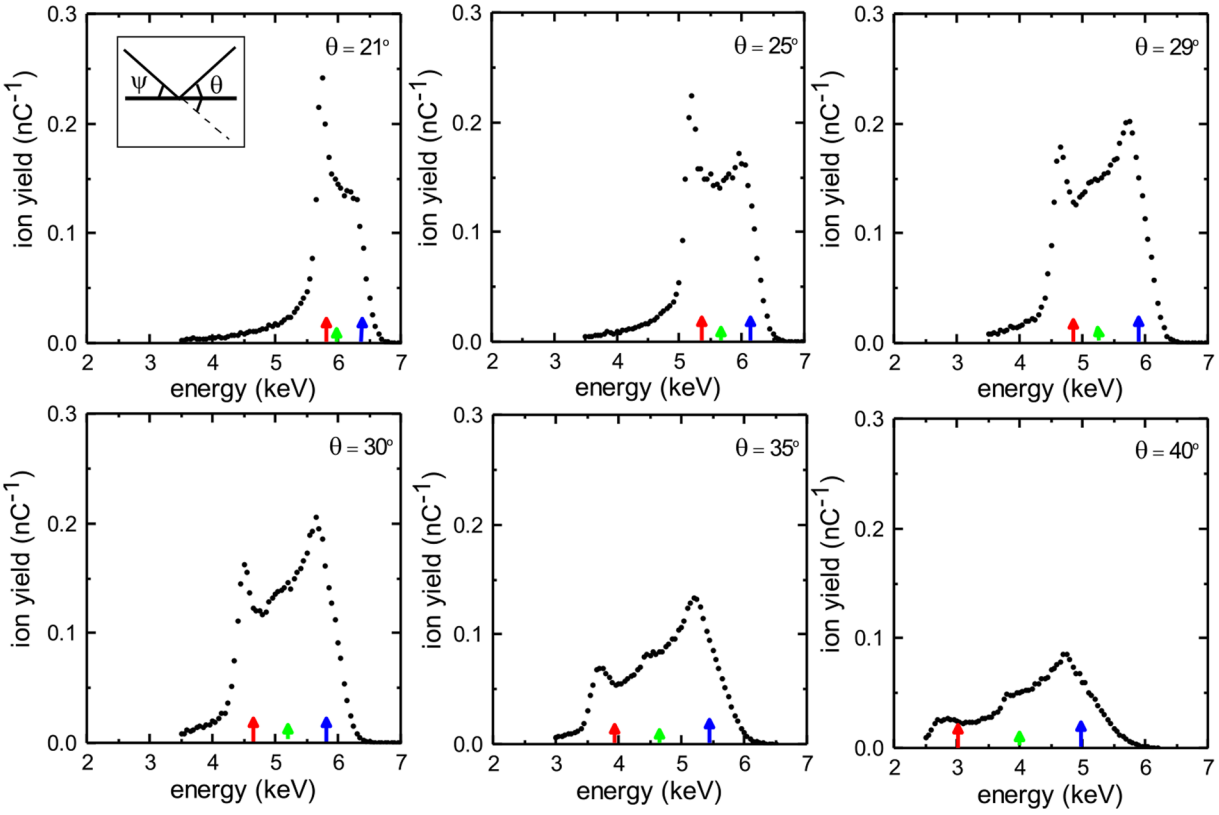

Fig. 1. Compilation of energy spectra of scattered 7 keV Kr^+ ions incident on a Cu target at an incidence angle ψ of 15°; the different plots show the spectrum for different scattering angles θ. The energy positions of single and symmetric double scattering are marked by red and blue arrows, respectively. The green arrows indicate the energy of primary Cu recoils. (For interpretation of the references to color in this figure legend, the reader is referred to the web version of this article.)

a linear background of multiple scattering events underlying the SC peak, as shown in the inset. The uncertainties in the experimental SC yields are assessed by taking realistic upper and lower linear backgrounds. The data from the SRIM simulation are scaled to the data point at 31°, because SRIM does not consider the charge state of the particles and thus the SRIM spectra can not be separated into individual ion and neutral contributions. The angular dependency predicted by SRIM is in good agreement with the experimental data. As can be seen, the SC ion yield is bell-shaped with its maximum at 30°.

Independent of the exact form of the interaction potential, for a two-body single collision, one expects the SC yield to increase towards smaller scattering angles, because of the increasing cross sections for smaller scattering angles [14,17]. However, in the experimental SC yield we see an opposite trend for angles smaller than 30°, the SC intensity decreases. It is to be realized that we solely measure the *ionic* SC yield. The lower SC yields at smaller scattering angles might be driven by a lower fraction of scattered ions. For smaller scattering angles, on the outgoing trajectory, the ions' velocity normal to the surface is lower and thus the time an ion needs to travel through the surface's selvedge becomes longer. This reduces the probability to escape from the surface as an ion, therefore ion fractions become smaller at lower scattering angles [16]. In addition, contributions to the SC peak from single-scattering off the second (and third, …) topmost layers will get less at smaller scattering angles as the probability for the particle to escape from the target without undergoing a second collision becomes smaller. The latter process is included in the SRIM simulations. Therefore in a comparison between SRIM and experimental results the particle-escape probability is included while the electronic processes are not. Unfortunately such a comparison for the SC yields is hampered by the fact that SRIM does not predict a SC peak at angles below 30°. Given that pure SC events mainly arise from the topmost layer, it is expected that changes in the ion fraction are more important than the changes in the particle-escape probabilities.

That expectation of significantly lower ion fractions at smaller scattering angles finds support in the trends observed in the total experimental ion yields depicted in Fig. 4. For scattering angles down from 30°, where the SC yield decreases by some 40% (see Fig. 3) the total scattered ion yield drops by a factor of 4. Therefore, the contribution of the SC peak to the ion spectrum increases rapidly towards smaller scattering angles.

To get some information on to what extent the drop in the total ion yield is due to changing ion fraction and not an overall reduction of the number of backscattered particles at scattering angles below 30°, a comparison is made to the total yields predicted by SRIM. As can be seen from Fig. 4 the total yields obtained from the SRIM simulations show significant reduction in their yields only for scattering angles below 24°. Based on small changes in the SRIM yields of tens of percent one may conclude that the reduction in the measured, total ion yields of a factor of 4 is by and large due to decreasing ion fractions.

A remarkable and noteworthy feature in the angular dependence of SRIM's total yield is an abrupt kink at 30°. This kink is likely due to the absence of a SC peak below 30° in the SRIM results. The SRIM yields in this angular range can be corrected for a missing SC contribution by extrapolating the SC fraction at angles larger than 30°. The SC fractions, which are calculated by dividing SC yields by total ion yields, are depicted in Fig. 5. The figure demonstrates that for angles larger than 30° SRIM predicts for 7 keV Kr an almost constant SC fraction (SCF) of approximately 0.15. Assuming that below 30° SRIM only misses out on the SC events, we have corrected the SRIM data in Fig. 4 for a missing SCF of 0.15 by multiplying the SRIM data by the factor 1/(1 - SCF). The SRIM data point at 30° is corrected for missing a SCF of 0.075 since we binned the SRIM data in angular bins of ± 1°. This implies that half of

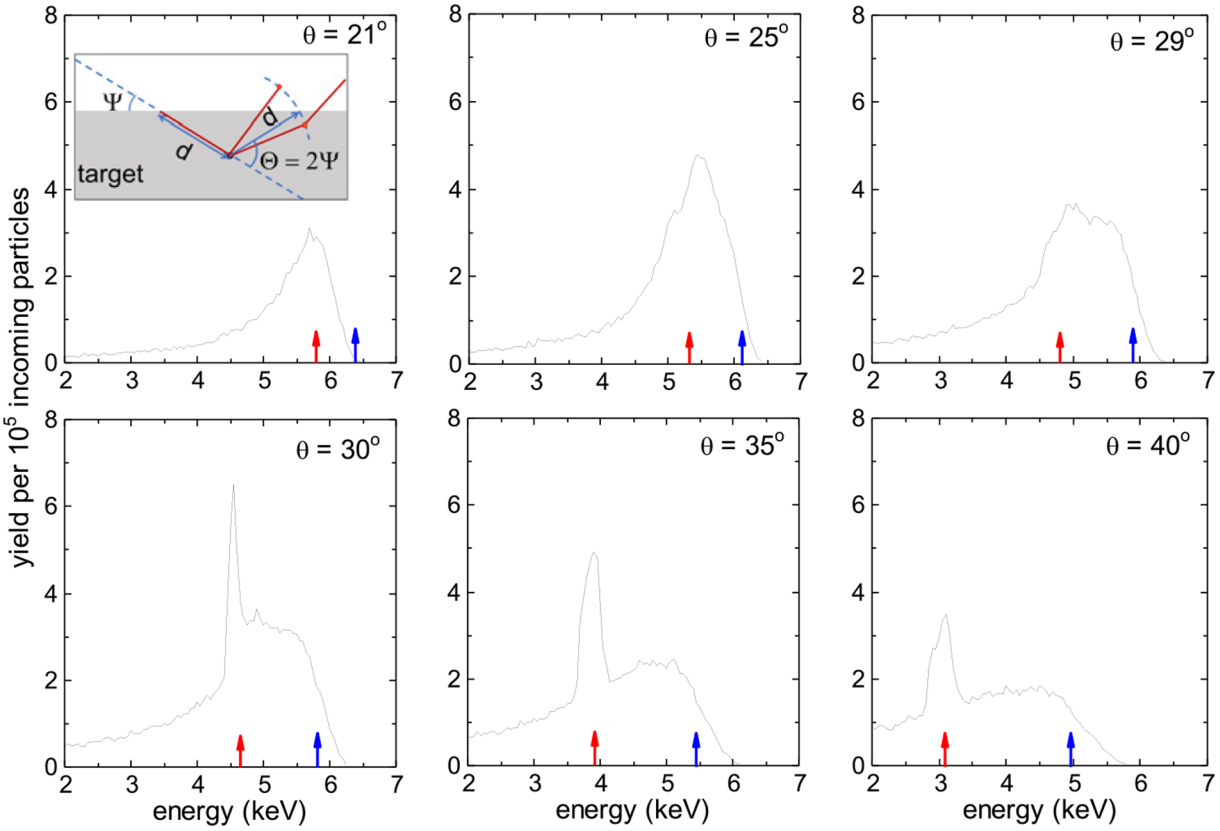

Fig. 2. Compilation of scattered energy distributions as simulated by SRIM for 7 keV Kr impinging on Cu at an incidence angle ψ of 15°; the different plots show the spectrum for different scattering angles θ. The energy positions of single and symmetric double scattering are marked by red and blue arrows, respectively. The inset shows a schematic explaining why single-collision scattering cannot occur in SRIM for scattering angles $\theta < 2\psi$. (For interpretation of the references to color in this figure legend, the reader is referred to the web version of this article.)

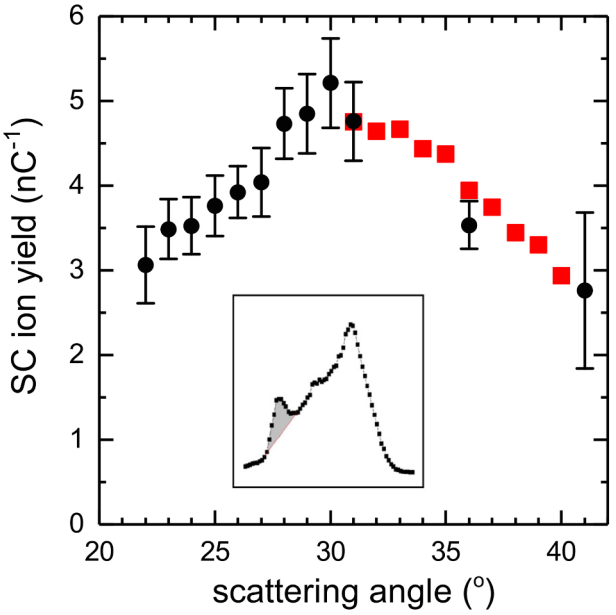

Fig. 3. Scattering-angle dependence of the single-collision ion yield (black symbols) for 7 keV Kr^+ ions on Cu at an incidence angle ψ of 15°. The closed red squares indicate yields obtained from SRIM (scaled at 31°). The inset shows how the SC yield is determined: by integrating the shaded area under the SC peak in the energy spectrum. (For interpretation of the references to color in this figure legend, the reader is referred to the web version of this article.)

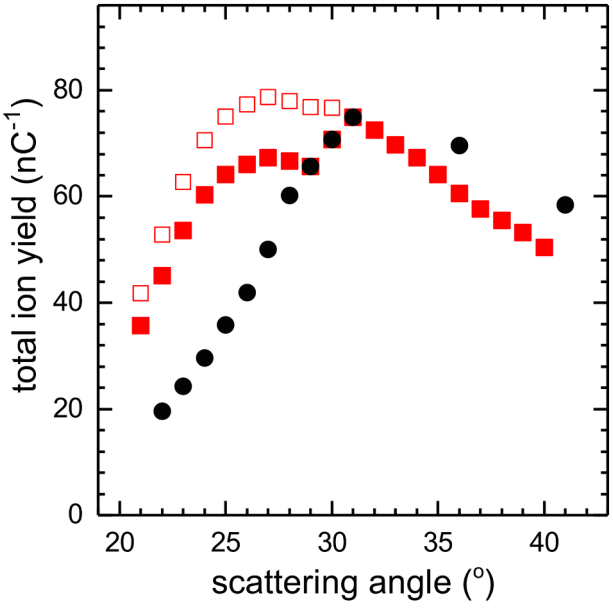

Fig. 4. Scattering-angle dependence of measured total ion yields (black symbols) for 7 keV Kr^+ ions on Cu at an incidence angle ψ of 15°. The closed red squares indicate total scattering yields obtained from SRIM (scaled at 31°), which at angles below 30° lack contributions from SC events.The open red squares show the SRIM data after correction for the missing SC events at angles below 30°. The correction is based on assuming a constant SC fraction (see Fig. 5). (For interpretation of the references to color in this figure legend, the reader is referred to the web version of this article.)

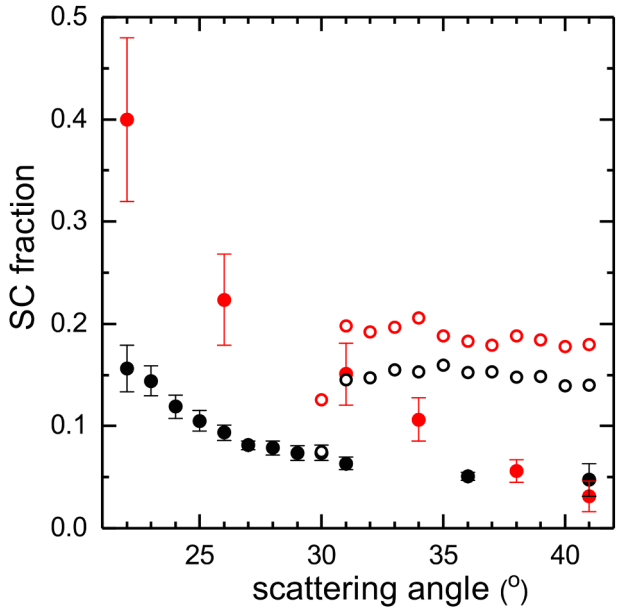

Fig. 5. Single-collision fractions of 7 (black) and 5 (red) keV Kr^+ impinging on Cu at an incidence angle ψ of 15°. The closed and open symbols represent the data from experiment and SRIM, respectively. (For interpretation of the references to color in this figure legend, the reader is referred to the web version of this article.)

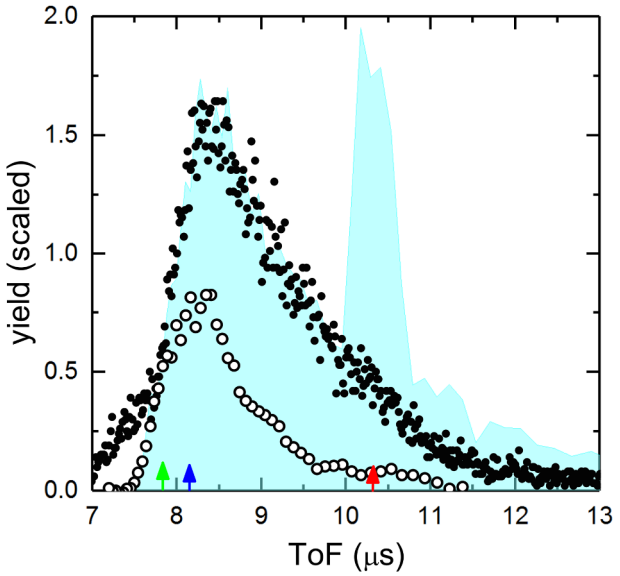

Fig. 6. Comparison of the experimental ToF spectrum (closed black symbols) of backscattered particles (ions and neutrals) and the SRIM predictions (cyan) for 5 keV Kr^+ ions on a Cu target at a scattering geometry of $(\psi, \theta) = (15°, 40°)$. The open black symbols represent the measured ion energy spectrum converted to time scale. The ToF positions of single and symmetric double scattering are marked by red and blue arrows, respectively. The green arrow indicates the position of primary Cu recoils in the ToF spectrum. (For interpretation of the references to color in this figure legend, the reader is referred to the web version of this article.)

the bin size is above 30° while the other half falls below 30°, so only for the latter half the correction is needed. Correcting the SRIM data in this manner fully removes the kink in the SRIM yields near 30° and nicely smoothens the SRIM data as a function of scattering angle.

The fact that SRIM predicts a constant SC fraction is a priori not expected since the largest part of the total yield is due to a variety of multiple-collision events of which many occur along longer trajectories through the target exposing them to additional energy loss by straggling. It seems thus unlikely that this wide ensemble of scattering events would have the same angular dependence as the single-collision events leading to the SC peak. For 7 keV Kr^+ ions the experimental data (see Fig. 5) do not exclude the SC fraction to be almost constant at scattering angles above 30°, though the experimental values are a factor of three smaller than the SRIM ones.

Next to the 7 keV experiments, we have performed some experiments at a lower energy of 5 keV Kr^+ ions which are shown in the same Fig. 5. The larger uncertainty associated with this 5-keV data is due to a much lower count rate, which is in line with a lower ionization fraction at lower velocities. Notwithstanding the larger uncertainties, the 5-keV data clearly shows a SC fraction that is not constant with angle, in contradiction with what SRIM predicts. At the smaller scattering angles, the SC fraction at 5 keV is about a factor of 2 larger than for 7 keV. In the SRIM simulations, the difference between 5 and 7 keV Kr ions is much smaller than in the experimental data, namely only 30%.

To verify whether SC scattering might be more prominent in the neutrals, a Time of Flight (ToF) measurement, which detects neutrals and ions alike, was performed at a scattering angle of 40° for 5 keV Kr^+ ions. The measured ToF spectrum is depicted in Fig. 6. The figure shows no clear sign of a SC peak (red arrow position). Therefore, the SC fraction is very small, which is in line with the small SC fraction of ~3% observed in the ionic measurements (cf. Fig. 5). Therefore the ToF data confirm the conclusion drawn from the ion data that there is a considerable difference (factor of ~3) between experiment and SRIM in the strength of the SC peak. Therefore, concerning the SC peak there is no appreciable difference between energy spectra of ions and neutrals and thus the ion data can be considered to be representative for the scattering of Kr ions from Cu.

Along with the ToF spectrum, the prediction of SRIM is also plotted in Fig. 6. The overall shape of the ToF spectrum simulated by SRIM is in good agreement with our experimental data except for the strong SC peak around 10.3 μs which is absent in the measurements. In addition it is noted that at shorter flight times around 7 to 8 μs, the ToF measurements show a gradual increase in intensity while SRIM predicts a steep rise from 7.6 μs on. The intensity below 8 μs stems from the contribution of primary Cu recoils to the ToF spectrum and not from fast Kr particles. As the ESA measurements of the kinetic energies of the ions are not sensitive to the mass of the ions, the Cu recoils will end up in between the SC and SDC energies in the ESA spectrum (see e.g. Fig. 1). Conversion of the ESA spectrum to ToF, assuming all ions to be Kr ions, should not exhibit any intensity at the shortest flight times. Therefore to verify the assignment of primary Cu recoils in the ToF spectrum in Fig. 6 we have added the results of an ESA measurement after converting the data from energy to time scale. The ESA spectrum is visually scaled to overlap SRIM and ToF spectrum at shorter flight times. It shows the same steep increase at shorter flight times as in the SRIM simulations, thereby it underlines the assignment of the ToF spectrum at the flight times below 8 μs to primary Cu recoils.

A further comparison of the shapes of the direct and converted ToF spectra indicates that beyond 8.5 μs the yields from the converted ESA spectrum drop faster than in the direct ToF measurements. This is another indication that at lower kinetic energies the ion fractions get lower. Therefore, a quantitative comparison of ion spectra to SRIM simulations requires accurate knowledge on ion fractions. However, as shown here by the comparison of the ESA (ions only) and ToF (neutrals and ions) spectra, not knowing the exact ion fraction does not inhibit one to draw conclusions on the presence or absence of the single-collision peak in the spectra.

4. Conclusions

The scattering of Kr ions off a Cu sample has been studied by means of ion scattering spectroscopy at incoming energies of 7 and 5 keV. The

mass ratio of Cu and Kr (≈0.8) is similar to that of Mo (or Ru) to Sn. Therefore, within a binary collision approximation the kinetics of single scattering is the same for Kr–Cu as it is for Sn–Mo. While for Sn ion scattering on Mo no single-collision (SC) peaks show up in the energy distribution of scattered ions, in the present study we find that they do for the lighter system of Kr ions on Cu. The presence of SC peaks and their angular dependence hints at the binary collision approximation being a viable approximation. The measured SC peaks decrease in intensity with increasing scattering angle. SRIM does not predict a SC contribution to the spectra at scattering angles smaller than twice the incoming angle, which is an imperfection of the code's algorithm of calculating subsequent binary collisions. For larger scattering angles SRIM predicts that the contribution of the SC peak to the spectra is constant at about 15%. However, at those larger scattering angles, the measured SC peaks continue to decrease and are weaker than predicted by SRIM by a factor of three. The measured angular dependence of the single-collision peaks, which is a signature of the scattering potential, could serve as a guide with which one can adjust SRIM to improve its description of low-energy heavy particle scattering off surfaces. For example, the generic ZBL-potential used by SRIM [4,5], which is based on the full range of energies and masses, might not be most suitable for such systems. An optimized potential could also be of benefit to the modelling of Sn ion collisions on Ru capping layers of EUV collecting mirrors in modern nanolithography tools.

Declaration of Competing Interest

The authors declare that they have no known competing financial interests or personal relationships that could have appeared to influence the work reported in this paper.

Acknowledgment

This work was carried out at the ZERNIKELEIF facility at the Zernike Institute for Advanced Materials of the University of Groningen as part of the research portfolio of the Advanced Research Center for Nanolithography, a public–private partnership between the University of Amsterdam, the Vrije Universiteit Amsterdam, the Netherlands Organization for Scientific Research (NWO), and the semiconductor equipment manufacturer ASML.

References

[1] M.J. Deuzeman, PhD thesis, University of Groningen (2019).
[2] S. Bajt, J.B. Alameda, T.W. Barbee, W.M. Clift, J.A. Folta, B.B. Kaufmann, E.A. Spiller, Opt. Eng. 41 (2002) 1797.
[3] Q. Huang, V. Medvedev, R. van de Kuijs, A. Yakshin, E. Louis, F. Bijkerk, Appl. Phys. Rev. 4 (2017) 011104.
[4] J.F. Ziegler, J.P. Biersack, U. Littmark, The Stopping and Range of Ions in Solids, Pergamon Press, New York, 1985.
[5] J. Ziegler, J. Biersack, M. Ziegler, SRIM – The Stopping and Range of Ions in Matter, SRIM Co, Chester, Maryland, 2008.
[6] J.F. Ziegler, M.D. Ziegler, J.P. Biersack, Nucl. Instrum. Methods Phys. Res. B 268 (2010) 1818.
[7] V.Y. Banine, K.N. Koshelev, G.H.P.M. Swinkels, J. Phys. D: Appl. Phys. 44 (2011) 253001.
[8] O.O. Versolato, Plasma Sources Sci. Technol. 28 (2019) 083001.
[9] A. Bayerle, M.J. Deuzeman, S. van der Heijden, D. Kurilovich, T. de Faria Pinto, A. Stodolna, S. Witte, K.S.E. Eikema, W. Ubachs, R. Hoekstra, O.O. Versolato, Plasma Sources Sci. Technol. 27 (2018) 045001.
[10] E. Bodewits, H.M. Dang, A.J. de Nijs, D.F.A. Winters, R. Hoekstra, Nucl. Instrum. Methods Phys. Res. B 267 (2009) 594.
[11] N. Stolterfoht, R. Hellhammer, D. Fink, B. Sulik, Z. Juhász, E. Bodewits, H.M. Dang, R. Hoekstra, Phys. Rev. A. 79 (2009) 022901.
[12] S.T. de Zwart, A.G. Drentje, A.L. Boers, R. Morgenstern, Surf. Sci. 217 (1989) 298.
[13] M. Krems, J. Zirbel, M. Thomason, R.D. DuBois, Rev. Sci. Instrum. 76 (2005) 093305.
[14] L.C. Feldman, J.W. Mayer, Fundamentals of Surface and Thin Film Analysis, Elsevier Science Publishing Co, New York, 1986.
[15] V.I. Shulga, Appl. Surf. Sci. 439 (2018) 456.
[16] H. Niehus, W. Heiland, E. Taglauer, Surf. Sci. Rep. 17 (1993) 213.
[17] W.K. Chu, J.W. Mayer, M.A. Nicolet, Backscattering Spectrometry, Academic Press, New York, 1978.